MOLECULAR IMAGING AND BIOLOGY

Mol Imaging Biol (2018)
DOI: 10.1007/s11307-018-1288-6

RESEARCH ARTICLE

[^{18}F]FE-OTS964: a Small Molecule Targeting TOPK for *In Vivo* PET Imaging in a Glioblastoma Xenograft Model

Giacomo Pirovano,[1] Sheryl Roberts,[1] Christian Brand,[1] Patrick L. Donabedian,[1] Christian Mason,[1] Paula Demétrio de Souza,[1] Geoff S. Higgins,[2] Thomas Reiner[1,3]

[1]*Department of Radiology, Memorial Sloan-Kettering Cancer Center, 1275 York Avenue, New York, NY, 10065, USA*
[2]*CRUK/MRC Oxford Institute for Radiation Oncology, University of Oxford, Oxford, UK*
[3]*Department of Radiology, Weill Cornell Medical College, New York, NY, USA*

Abstract

Purpose: Lymphokine-activated killer T cell-originated protein kinase (TOPK) is a fairly new cancer biomarker with great potential for clinical applications. The labeling of a TOPK inhibitor with F-18 can be exploited for positron emission tomography (PET) imaging allowing more accurate patient identification, stratification, and disease monitoring.

Procedures: [^{18}F]FE-OTS964 was produced starting from OTS964, a preclinical drug which specifically binds to TOPK, and using a two-step procedure with [^{18}F]fluoroethyl p-toluenesulfonate as a prosthetic group. Tumors were generated in NSG mice by subcutaneous injection of U87 glioblastoma cells. Animals were injected with [^{18}F]FE-OTS964 and PET imaging and *ex vivo* biodistribution analysis was carried out.

Results: [^{18}F]FE-OTS964 was successfully synthesized and validated *in vivo* as a PET imaging agent. The labeling reaction led to 15.1 ± 7.5 % radiochemical yield, 99 % radiochemical purity, and high specific activity. Chemical identity of the radiotracer was confirmed by co-elution on an analytical HPLC with a cold-labeled standard. *In vivo* PET imaging and biodistribution analysis showed tumor uptake of 3.06 ± 0.30 %ID/cc, which was reduced in animals co-injected with excess blocking dose of OTS541 to 1.40 ± 0.42 %ID/cc.

Conclusions: [^{18}F]FE-OTS964 is the first TOPK inhibitor for imaging purposes and may prove useful in the continued investigation of the pharmacology of TOPK inhibitors and the biology of TOPK in cancer patients.

Key words: Molecular imaging, Glioblastoma, TOPK, PET, OTS964

Introduction

Lymphokine-activated killer T cell-originated protein kinase (TOPK), also known as PDZ-binding kinase (PBK), is a Ser/Thr protein in the mitogen-activated protein kinase-kinase family with a role in regulation of proliferation and cell cycle progression [1–3]. TOPK is overexpressed in a significant fraction of clinical cases of many cancer types, including breast [4], colorectal [5], leukemia and lymphoma [6, 7], ovarian [8], lung [9, 10], glioma [11, 12], and high TOPK expression correlates with poor prognosis, invasiveness, and propensity to form metastases [8, 9, 13–15]. In cancer cell lines, disruption of TOPK causes cytokinesis defects [16], chemosensitization [17], and radiosensitization

Electronic supplementary material The online version of this article (https://doi.org/10.1007/s11307-018-1288-6) contains supplementary material, which is available to authorized users.

Correspondence to: Thomas Reiner; *e-mail:* reinert@mskcc.org

Published online: 24 October 2018

by altering the G_2/M checkpoint and increasing apoptosis [18]. TOPK overexpression into normal epithelial cells causes transformation *in vitro* and *in vivo* [5]. TOPK is considered to be a "consensus stemness ranking signature" gene in glioblastoma [19]. Furthermore, human TOPK is minimally expressed in normal adult tissues outside the testis, though it is highly expressed in placenta and many fetal tissues [20]. In mice, the TOPK ortholog is found to be expressed mainly in the central nervous system and liver. Despite more is yet to be discovered about the mechanisms underlying a role for TOPK in cancer development and susceptibility to curative therapy, its cancer-specific presence and its function make TOPK both an attractive target for drug discovery and a valuable cancer biomarker.

Based on the cancer specificity of TOPK expression, a radiolabeled TOPK inhibitor with the positron-emitting isotope F-18 could be used to image and monitor malignancies. First-generation drugs have been developed to specifically inhibit TOPK: HI-TOPK-032 (IC_{50} of 2 μM) [21], OTS514 (IC_{50} of 1.5 to 14.0 nM) and OTS964 (IC_{50} of 7.6 to 73.0 nM) [22], and ADA-07 [23]. Furthermore, pantoprazole and ilaprazole, two proton pump inhibitors, have been recently shown to target TOPK as well [24, 25]. Each of these compounds has been shown to specifically inhibit TOPK over other kinases and/or exhibit TOPK-dependent cell growth inhibition and has shown promising preclinical results in animal models. None of these TOPK inhibitors has yet entered clinical trials apart for OTS514, which has been tested in a phase I trial in acute myelogenous leukemia. Because of more detailed quantitative pharmacological data available and an extensive published structure-activity relationship (SAR) [8, 22, 26, 27], we chose to pursue labeling OTS514 and OTS964, which are identical except for the methylation of an amino group (Fig. S1, see Electronic Supplementary Material (ESM)). We decided to use a subcutaneous glioblastoma xenograft model due to the known high TOPK expression levels in glioblastoma [11, 19]. The U87 cell line was chosen due to its high levels of TOPK expression. Here, we report the synthesis and characterization of [^{18}F]FE-OTS964, the first radiolabeled molecule for non-invasive interrogation of TOPK expression *in vivo*.

Materials and Methods

General

Chemicals were procured from commercial suppliers and used without further purification. 4,7,13,16,21,24-Hexaoxa-diazabicyclo[8.8.8]hexacosane (K_{222}), dry dimethyl sulfoxide (DMSO) over molecular sieves, dry acetonitrile over molecular sieves, ethylene glycol ditosylate, potassium carbonate, and miscellaneous chemicals were purchased from Sigma-Aldrich (St. Louis, MO). 2-Fluoroethyl *p*-toluenesulfonate was purchased from TCI Chemicals America (Portland, OR). (*R*)-9-(4-(1-(dimethylamino)propan-2-yl)phenyl)-8-hydroxy-6-methylthieno[2,3-*c*]quinolin-4(5*H*)-one (OTS964) and (*R*)-9-(4-(1-aminopropan-2-yl)phenyl)-8-hydroxy-6-methylthieno[2,3-*c*]quinolin-4(5*H*)-one (OTS514) were purchased from Selleck Chemicals (Houston, TX). Water (> 18.2 MΩ cm^{-1} at 25 °C) was obtained from an Alpha-Q Ultrapure water system from Millipore (Bedford, MA). High-performance liquid chromatography (HPLC) purification and analysis was performed on a Shimadzu UFLC HPLC system with a DGU-20A degasser, an SPD-M20A UV detector, an LC-20AB pump unit, and a CBM-20A communication bus module, with a LabLogic Scan-RAM radio-TLC/radio-HPLC detector set up to detect radioactive signal. All HPLC purification was carried out on a semi-preparative HPLC (Phenomenex Gemini C18, 5 μm, 10 × 250 mm, 3.5 ml/min 5–95 % water/acetonitrile 18 min linear gradient, unless otherwise specified). LC-MS was performed on a Shimadzu LCMS-2020 (O1094900283SA) using a Water Atlantis T3 column (C18, 5 μm, 4.6 mm × 100 mm). Nuclear magnetic resonance analysis was performed on a Bruker 500 MHz spectrometer at the Memorial Sloan-Kettering Nuclear Magnetic Resonance Core Facility. All averages are presented as mean ± standard deviation. Doses of radiopharmaceuticals are expressed as decay-corrected to time of image acquisition. All injected dose calibrations for positron emission tomography (PET) images and biodistribution were corrected for partial paravenous administration by removing decay-corrected activity remaining in the tail after 1.25 h from the original estimate of injected dose. All animal experiments were performed in accordance with protocols approved by the Institutional Animal Care and Use Committee of Memorial Sloan Kettering Cancer Center (MSK) and followed the National Institutes of Health guidelines for animal welfare.

Chemistry

Synthesis of (*R*)-9-(4-(1-(dimethylamino)propan-2-yl)phenyl)-8-(2-fluoroethoxy)-6-methylthieno[2,3-*c*]quinolin-4(5*H*)-one ([^{19}F]FE-OTS964). OTS964 (14 mg, 0.03 mmol), 2-fluoroethyl *p*-toluenesulfonate (12 μl, 15 mg, 0.07 mmol), Cs_2CO_3 (13 mg, 0.04 mmol), and dry DMSO (200 μl) were added to a nitrogen-flushed 4-ml vial along with a stir bar. The vial was flushed with nitrogen again, sealed, and heated to 60 °C for 1 h. After removal of DMSO by lyophilization, the residue was extracted with CH_2Cl_2 and saturated sodium bicarbonate, the organic phase dried under gentle nitrogen and fractionated on semi-preparative HPLC to yield [^{19}F]FE-OTS964 (1 mg, 6.4 % yield) after lyophilization as a white solid. Purity: 99 % by analytical HPLC. t_R = 14.4 min. ^{1}H NMR of *O*-alkylated OTS964. ^{1}H NMR (DMSO-d6, 600 MHz): δ 10.78 (s, 1H, –N(CH_3)$_2$H$^+$), 9.19 (s, 1H, Ar-NH), 7.63 (d, *J* = 5.4 Hz, 1H, –CHCHS), 7.45–7.39 (m, 2H, –CH^{Ar}), 7.26 (s, 1H, –CH^{Ar}), 7.22–7.15 (m, 2H, –CH^{Ar}), 5.73 (d, *J* = 5.4 Hz, 1H, –CHCHS), 4.42 (ddd, *J* = 47.8, 7.5, 3.8 Hz, 2H, –OCH$_2$CH$_2$F), 4.13 (ddd,

J = 30.2, 4.5, 3.2 Hz, 2H, –OC$\underline{H}_2$CH$_2$F), 3.46–3.36 (m, 3H, Ar-C$\underline{H}$(CH$_3$)C$\underline{H}_2$–), 2.76 (dd, J = 28.7, 4.8 Hz, 6H, –N(C$\underline{H}_3$)$_2$), 2.51 (s, 3H, Ar-C$\underline{H}_3$), 1.31 (d, J = 6.7 Hz, 3H, –C$\underline{H}_3$). Identity by LC-MS analysis, ESI-MS (ES$^+$) calculated for $C_{25}H_{27}FN_2O_2S$ $[M + H]^+$ m/z 439.4, found 439.18.

Radiochemistry

No-carrier-added [^{18}F]fluoride was produced by the ^{18}O(p,n)^{18}F reaction of 16.5 MeV proton incident on an O-18 enriched water target in a GE Healthcare PETTrace 800 cyclotron. To separate the [^{18}F]fluoride in a form suitable for nucleophilic fluorination, the ^{18}O-enriched water containing [^{18}F]fluoride was passed through an anion-exchange cartridge (Waters Sep-Pak QMA Light), which was then eluted with 2 ml of 11.95 mM K_{222} and 20 mM K_2CO_3 in 4 % H_2O/acetonitrile into a kiln-dried V-vial. Water was removed azeotropically by heating at 120 °C under a gentle stream of nitrogen until almost no visible liquid remained. Subsequent radiosynthesis of [^{18}F]FE-OTS964 was completed in two steps, using two HPLC purification steps to ensure high chemical and radiochemical purity and specific activity at each step. 2-[^{18}F]Fluoroethyl *p*-toluenesulfonate was prepared in dry acetonitrile (500 µl) by adding ethylene glycol ditosylate (5 mg) to the vial used to dry the [^{18}F]fluoride. The vial was sealed, heated to 110 °C for 6 min under stirring, then cooled to room temperature, diluted with 500 µl of water, and purified on semi-preparative HPLC. The collected peak (16 min) containing 2-[^{18}F]fluoroethyl *p*-toluenesulfonate was diluted 10:1 with 35 % ethanol, trapped on a Waters HLB Sep-Pak Plus, and eluted with 500 µl dry acetonitrile into the second reaction vessel already containing K_2CO_3 (3 mg) and stir bar. OTS964 (2 mg) was added as suspension in dry DMSO (100 µl) and heated to 120 °C. After 10 min, 30 µl of 1 N HCl was added; the solution was diluted with 1 ml of water and purified on HPLC. The collected peak (14 min) was diluted 10:1 with water, trapped on a Waters C18 Sep-Pak Light cartridge, eluted with 400 µl of ethanol, and diluted to < 5 % ethanol with sterile normal saline, affording [^{18}F]FE-OTS964 in 15.1 ± 7.5 % overall decay-corrected radiochemical yield (based on measuring isolated final product on a dose calibrator at the end of formulation), 99 % radiochemical purity, and molar activity of > 15 GBq/µmol. No decomposition of the tracer was noted either *in vitro* or *in vivo*, suggesting sufficient stability. Synthesis was performed manually, starting with 150 mCi of [^{18}F]fluoride as delivered by the cyclotron; radiochemical yields are calculated from the activity eluted from the anion exchange cartridge. The fraction collected during the first HPLC run (containing 2-[^{18}F]fluoroethyl p-toluenesulfonate) was approx. 5 ml, and that collected during the second HPLC run (containing [^{18}F]FE-OTS964) was approx. 4 ml. Yield of the first step was 51–60 %. For the solid phase cartridges: QMA Light 0 % flow-through 5–30 % retention; HLB Plus 10 % flow-through 0 % retention; C18 light 0 % flow-through 10 % retention. Cold chemistry was performed under different conditions leading to three different products (Supplementary Information). Synthesis was completed within 1.5 half-lives from EOB. Final activity of labeled compound was 3–6 mCi. Specific activity is corrected to EOS.

Cell Culture

U87 cells were kindly provided by Dr. Vladimir Ponomarev. Cells were maintained in 150-cm^2 tissue culture flasks in Eagle's modified essential medium supplemented with 10 % heat-inactivated fetal bovine serum, 100 IU/ml penicillin, and 100 µg/ml streptomycin, stored in a cell culture incubator at 37 °C and 5 % CO_2 atmosphere, changing media every 2 days and passaging at 70 % confluence.

Animal Models

To generate mice with U87 tumors, 20- to 24-week-old NOD *scid* gamma (NOD.Cg-*Prkdc*^{scid}*Il2rg*^{tm1Wjl}/SzJ, n = 6, Jackson Laboratory, Bar Harbor, ME) mice were anesthetized with 2 % isoflurane in 2 l/min medical air, the right flank depilated and 1×10^6 U87 cells in 150 µl of 1:1 cell culture media/Matrigel (Corning, Corning, NY) were injected subcutaneously. Tumors were allowed to proliferate for 3 weeks and reached a size of 50–100 mm^3.

Immunoblotting

To generate tissue whole protein extracts, organs were surgically resected from tumor-bearing mice and incubated in RIPA buffer with protease inhibitors. Tissue was then lysed using a tissue homogenizer (OMNI GLH International) at 4 °C for 1 min. Lysates were run on a SDS-Page gel (BioRad). Bound antibodies were detected by developing film from nitrocellulose membranes exposed to chemiluminescence reagent. Antibodies: anti-TOPK (Sigma SAB5300406 clone 2C8, 1:1000), monoclonal mouse antibody, human reactive; anti-Vinculin (Abcam ab18058, 1:500).

Blood Half-Life

Blood half-life determination was performed in tumor-bearing mice which received 34–41 µCi of [^{18}F]FE-OTS964 (formulated in 50 µl, < 5 % ethanol in sterile normal saline) *via* injection into the retroorbital sinus under 2 % isoflurane anesthesia delivered *via* nose cone in 2 l/min medical air. Immediately after tracer injection, mice were allowed to recover from anesthesia, and blood was drawn at appropriate timepoints by pricking the tail vein with a sterile

27.5 G needle and collecting blood using a previously weighed, heparin-coated glass capillary. Capillaries were weighed, activity counted on a gamma-counter (Wizard^2 3″ 2480, Perkin-Elmer, Waltham, MA) with internal fluorine-18 standards, and the data converted to %ID/g. Blood half-life data was processed by fitting a monoexponential decay function constrained to reach a plateau at $y = 0$.

PET Imaging and Biodistribution

PET imaging was performed on a Focus 120 microPET (Concorde Microsystems, Knoxville, TN), with animals under 2 % isoflurane anesthesia delivered *via* nose cone in 2 l/min medical air. A total of five mice were imaged for the study. The same animals were sacrificed after imaging for biodistribution analysis. After acquisition (10 min with >20 million counts/scan), list mode emission data were sorted into two-dimensional sinograms *via* Fourier rebinning; data were normalized to correct for non-uniform detector response, deadtime count losses, and positron branching ratio, but no attenuation, scatter, or partial-volume averaging corrections were applied. Sinogrammed data were reconstructed into a 128 × 128 × 95 matrix (0.87 × 0.87 × 0.77 mm voxel size) by filtered back-projection. Image counts per voxel per second were converted to activity concentrations (%ID/cc) using a system-specific calibration factor derived from imaging a mouse-sized water-equivalent phantom containing fluorine-18. Reconstructed data were processed and VOIs drawn using Inveon Research Workplace software (Siemens). After image acquisition, mice were sacrificed, their organs dissected into previously weighed culture tubes, the tubes weighed, activity counted on a gamma-counter (Wizard^2 3″ 2480, Perkin-Elmer, Waltham, MA) with internal fluorine-18 standards, and the data converted to %ID/g.

Results

Synthesis

We chose to pursue [^{18}F]fluoroethylation at the phenol oxygen on OTS964 (Fig. 1), since the published SAR indicated that conversion of this group to an alkyl ether did not perturb TOPK-dependent cell growth inhibition [26] (Fig. S2, see ESM). We confirmed the chemical identity of all three products by HPLC, LC-MS, and NMR (Figs. S3 to S8, see ESM). The synthesis produced three different products: (i) *O*-alkylated OTS964, (ii) *N*-alkylated OTS964, and (iii) *O*-,*N*-alkylated OTS964. Fluoroethylation of OTS964 with 2-fluoroethyl *p*-toluenesulfonate produced the desired [^{19}F]FE-OTS964 in 6.4 % yield. [^{19}F]FE-OTS964 eluted at 14.4 min, OTS964 eluted at 12.09 min on reverse phase HPLC, indicating good separation between the starting material and the product.

Production of radiolabeled [^{18}F]FE-OTS964 was completed following the well-established procedure of [^{18}F]fluoroethylation with 2-[^{18}F]fluoroethyl *p*-toluenesulfonate [28]. Production of [^{18}F]FE-OTS964 was accomplished in two steps (see QC chromatograms for production of 2-[^{18}F]fluoroethyl *p*-toluenesulfonate in Fig. S9 in ESM) with two HPLC purifications to ensure high purity and molar activity at each step. The synthesis was completed with 15.1 ± 7.5 % overall radiochemical yield, with 99 % radiochemical purity and acceptable molar activity. [^{18}F]FE-OTS964 co-eluted with [^{19}F]FE-OTS964 at 14.4 min on analytical HPLC, confirming their chemical identity (Fig. 2 and Fig. S6 in ESM).

Biochemistry

To demonstrate differential target expression underlying the possible high tumor-to-background ratios achievable with TOPK imaging, we performed *ex vivo* immunoblotting of

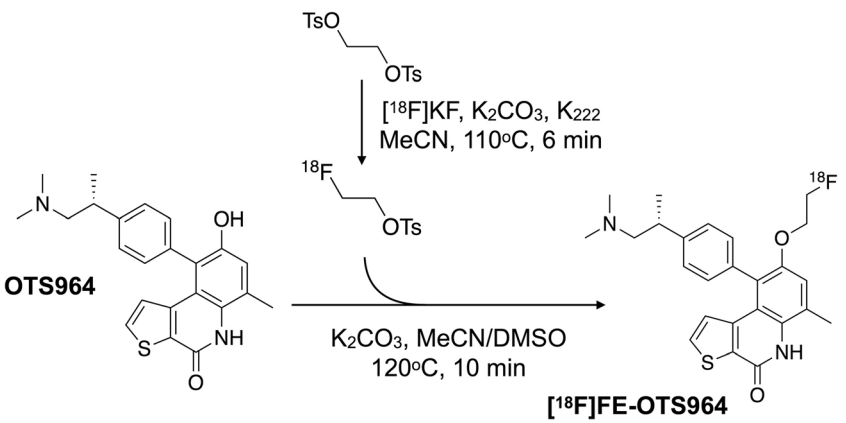

Fig. 1. Scheme for radiochemical synthesis. [^{18}F]FE-OTS964 was prepared by labeling OTS964 with 2-[^{18}F]fluoroethyl *p*-toluenesulfonate in a two-step reaction.

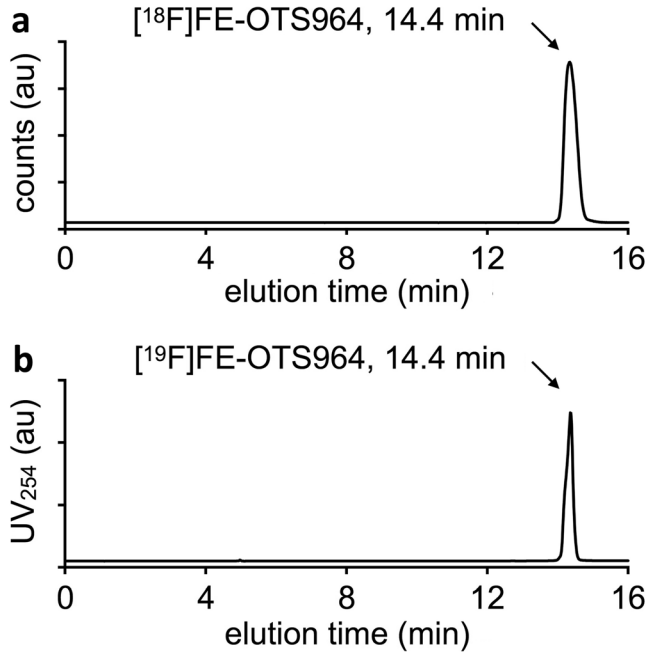

Fig. 2. Confirmation of chemical identity of [^{18}F]FE-OTS964 by analytical HPLC using a verified cold standard. **a** Radio-HPLC chromatogram of [^{18}F]FE-OTS964; **b** UV-HPLC chromatogram of [^{19}F]FE-OTS964; elution of both compounds at 14.4 min indicates identical chromatographic properties.

human TOPK using tissue from xenografted mice and U87 cultured cell protein extracts (Fig. S10 in ESM). No detectable human TOPK expression was found in the liver, lung, spleen, or kidney, but was detected in both cultured U87 cells and U87 xenografts.

PET Imaging, Biodistribution, and Specificity

PET imaging (Fig. 3, complete images in Fig. S11 and complete tabular VOI data in Table S1 in ESM) 1 h post-injection showed that regions of highest uptake were in the tumor, with unspecific uptake in the gallbladder, intestinal tract, spleen, and bladder, indicating mixed hepatobiliary and renal clearance. These findings were confirmed by *ex vivo* biodistribution (Fig. 4a, complete tabular data in Table S2, ESM). Mean tumor uptake of [^{18}F]FE-OTS964 as determined by VOI quantification of PET images was 3.06 ± 0.30 %ID/cc, reduced in blocked animals to 1.40 ± 0.42 %ID/cc ([^{18}F]FE-OTS964 + 5 mg/kg OTS514). *Ex vivo* biodistribution analysis determined mean tumor uptake of [^{18}F]FE-OTS964 as 3.59 ± 0.27 %ID/g, reduced in blocked animals to 1.61 ± 0.002 %ID/g. Uptake of liver was 5.61 ± 1.30 %ID/g, spleen 16.0 3.67 %ID/g, small intestine 6.66 1.89 %ID/g, large intestine 4.73 ± 0.45 %ID/g, and kidney 5.59 0.68 %ID/g. Uptake in the clearing organs was not specific as no statistically significant difference between animals administered [^{18}F]FE-OTS964 and animals administered an excess dose [^{18}F]FE-OTS964 + 5 mg/kg OTS514 was detected; *p* values for unblocked *vs* blocked organs being 0.342 for heart (*ns*), 0.159 for liver (*ns*), 0.382 for spleen (*ns*), 0.161 for muscle (*ns*), and 0.505 for bone (*ns*), except for kidney uptake, which was reduced in blocked animals to 3.36 ± 0.15 %ID/g (0.022 *p* value). Bone uptake was 2.6 ± 1.0 %ID/g in unblocked animals, without a statistically significant change in blocked animals.

Blood Half-Life

To determine the feasibility of [^{18}F]FE-OTS964 as an imaging agent and validate choice of imaging timepoint, we determined its blood half-life in NSG mice (Fig. 4b). [^{18}F]FE-OTS964 was found to clear blood quickly with a monophasic half-life of 8.5 min.

Discussion

TOPK is a cancer biomarker that has recently raised increasing interest in the scientific community due to its multi-faceted role in cancer development, aggressiveness, and response to treatment as well as a potential predictor of therapeutic efficacy. In this study, we established the feasibility of a radiolabeled TOPK inhibitor as an imaging agent for TOPK-expressing tumors. The rationale behind that is the convenient tumor-to-normal tissue differential expression of TOPK. Tissue Western blots *ex vivo* confirmed absence of TOPK expression in healthy tissues from normal adult mice, as opposed to detectable protein levels in tumor xenografts. Using 2-[^{18}F]fluoroethyl *p*-toluenesulfonate as a prosthetic group, we sought to label the molecule without reducing its binding specificity. We determined on the basis of a published SAR that labeling on the phenol (–OH) would allow the molecule to retain its affinity and selectivity for TOPK.

Synthesis was successful and produced three different products: (i) *O*-alkylated OTS964, (ii) *N*-alkylated OTS964, and (iii) *O*-,*N*-alkylated OTS964; however, optimizations remain to be performed to improve production of [^{18}F]FE-OTS964 on an efficient routine basis. Screening combinations of base and solvent conditions could improve the yield of [^{18}F]fluoroethylations with 2-[^{18}F]fluoroethyl *p*-toluenesulfonate [28]. It may also be possible to improve the synthesis process by first conjugating ethylene glycol ditosylate to the inhibitor and perform the last one step of the F-18 labeling on the following day. This would increase purity of the final product and overcome the limitations of working with short half-life radioactive material. Another possibility is to adapt to a one-pot format with a single HPLC purification separating [^{18}F]fluoroethylated from tosylethylated material. [^{18}F]FE-OTS964 cleared from the blood quickly and accumulated in tumors to a level of 3.06 ± 0.30 %ID/cc as measured *in vivo* by PET and 3.56 ± 0.27 %ID/g as measured by *ex vivo* biodistribution. The

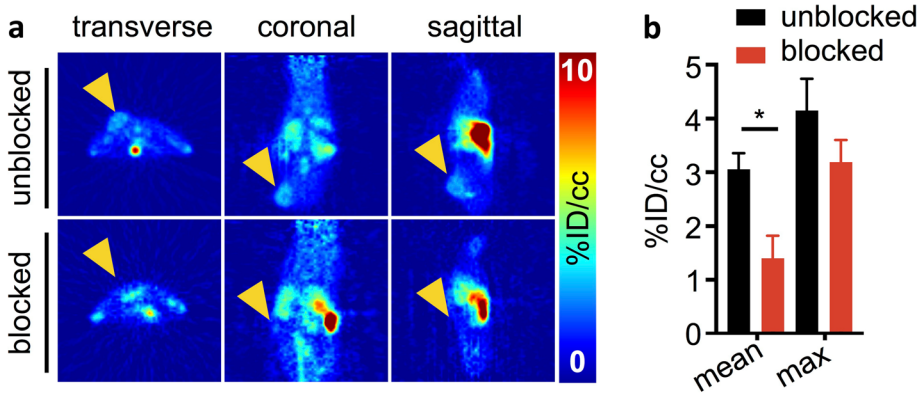

Fig. 3. *In vivo* PET imaging of [^{18}F]FE-OTS964 in U87 tumor-bearing NSG mice. **a** PET images (left to right: transverse, coronal, and sagittal) centered on the tumor in top (unblocked) mice injected with [^{18}F]FE-OTS964 and bottom (blocked) mice injected with [^{18}F]FE-OTS964 + 5 mg/kg OTS514. Arrows indicate tumor location. **b** VOI quantification of PET scans. Statistically significant differences were seen in mean voxel %ID/cc between blocked (black circles) and unblocked (red squares) mice. *Significant at $p < 0.05$.

lower measured values for PET are consistent with spill-out effects reducing apparent activity concentrations within the tumor. Reduction of tumor uptake with co-administration of a blocking dose reduced tumor uptake significantly, with tumor-to-muscle ratios falling from 2.14 ± 0.07 in unblocked animals to 1.24 ± 0.0002 in blocked animals. Blocking-dependent changes in blood and kidney uptake are likely due to confounding hematological toxicity of the blocking dose, as OTS514 at a dose of 5 mg/kg has been shown to induce leukocytopenia with thrombocytosis [22]. Nonspecific bone uptake of 2.56 ± 0.99 %ID/g, which can also be seen in the PET images, indicates a limited degree of *in vivo* defluorination.

PET imaging also shows unspecific uptake in the intestines, liver, kidneys, and spleen, which might be due to excretion of the molecule. This is also supported by the inability of detecting human TOPK expression using *ex vivo* immunoblotting. However, further studies on the anti-TOPK antibody need to be conducted in order to exclude its inability to detect mouse TOPK ortholog expression, even though this should not be a problem in a clinical setting, as TOPK tumor specificity has been documented in the past in humans. Another explanation for unspecific effect of the blocking agent in the kidneys could be the observed levels of blocking in the blood (p values of 0.022 and 0.011 for kidneys and blood, respectively). Hematopoietic cell toxicity has been previously demonstrated with TOPK inhibitors and could be circumvented by liposomal formulation and delivery [22].

Despite these issues, [^{18}F]FE-OTS964 should prove to be a good starting point for developing a noninvasive TOPK imaging platform. From here, we will develop a TOPK inhibitor library and select promising tracers based on affinity, pharmacokinetics, and target residence times. It is

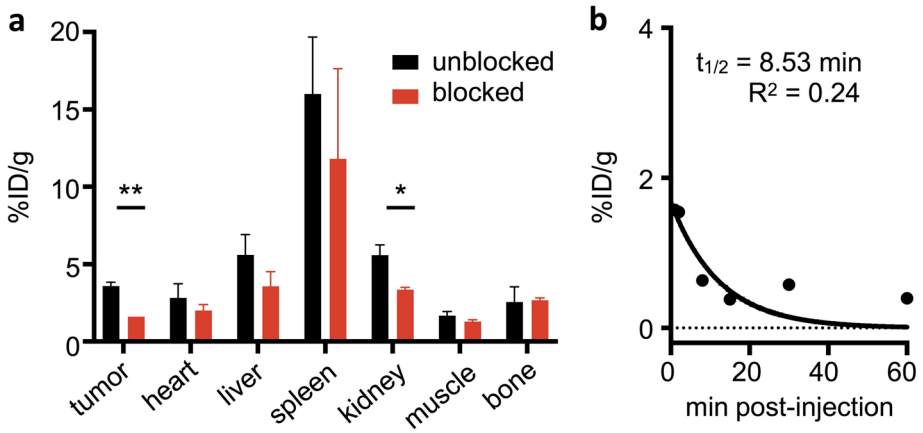

Fig. 4. *In vivo* biodistribution, specificity, and pharmacokinetics of [^{18}F]FE-OTS964. **a** Representative data of gamma-counting biodistribution analysis of mice injected with 71–141 μCi [^{18}F]FE-OTS964 (unblocked, black bars) or 51–60 μCi [^{18}F]FE-OTS964 + 5 mg/kg OTS514 (blocked, red bars). **b***In vivo* blood half-life of [^{18}F]FE-OTS964 in NSG mice. *Significant at $p < 0.05$, **significant at $p < 0.005$.

possible to speculate that, due to the tumor specificity of TOPK expression and its increasingly central role in the understanding of the many mechanisms underlying cancer development, invasion, and therapy resistance, TOPK could be an excellent candidate for broad imaging applications. These would include *in vivo* PET imaging as well as optical imaging with the potential of developing a clinically applicable tool for improved diagnosis.

Conclusion

In the present study, we produced and characterized [^{18}F]FE-OTS964, a F-18 labeled tracer for TOPK expression based on OTS964, a first-generation, selective inhibitor of TOPK. Specific uptake was observed in tumor, with favorable tumor-to-muscle ratios. [^{18}F]FE-OTS964 represents the first step toward noninvasive assessment of this highly promising biomarker. This study is the first step toward a clinically translatable radiolabeled TOPK inhibitor that may prove useful in unraveling the biology of TOPK and the pharmacology of its inhibitors.

Acknowledgements. The authors wish to acknowledge the support of Memorial Sloan Kettering Cancer Center's Animal Imaging Core Facility, Radiochemistry & Molecular Imaging Probes Core Facility, Integrated Genomics Core Facility, Nuclear Magnetic Resonance Core Facility, Media Preparation Core Facility, and Molecular Cytology Core Facility. We wish to thank Dr. Pat Zanzonico and Ms. Valerie Longo for technical support with PET/CT imaging, Mr. Sherron Hicks and Mr. Yorann Roux for operating the cyclotron, and Dr. Lukas Carter for helpful discussions.

Funding Information. This work was supported by National Institutes of Health grants R01 CA204441 (T.R.), P30 CA008748, and the Memorial Sloan Kettering Imaging and Radiation Sciences Program (T.R.).

Compliance with Ethical Standards. All animal experiments were performed in accordance with protocols approved by the Institutional Animal Care and Use Committee of Memorial Sloan Kettering Cancer Center (MSK) and followed the National Institutes of Health guidelines for animal welfare.

Conflict of Interest

TR and CB are co-founders and shareholders of Summit Biomedical Imaging, LLC.
The other authors declare that they have no conflicts of interest.

References

1. Abe Y, Matsumoto S, Kito K, Ueda N (2000) Cloning and expression of a novel MAPKK-like protein kinase, lymphokine-activated killer T-cell-originated protein kinase, specifically expressed in the testis and activated lymphoid cells. J Biol Chem 275:21525–21531
2. Gaudet S, Branton D, Lue RA (2000) Characterization of PDZ-binding kinase, a mitotic kinase. Proc Natl Acad Sci U S A 97:5167–5172
3. Shinde SR, Gangula NR, Kavela S, Pandey V, Maddika S (2013) TOPK and PTEN participate in CHFR mediated mitotic checkpoint. Cell Signal 25:2511–2517
4. Park JH, Lin ML, Nishidate T, Nakamura Y, Katagiri T (2006) PDZ-binding kinase/T-LAK cell-originated protein kinase, a putative cancer/testis antigen with an oncogenic activity in breast cancer. Cancer Res 66:9186–9195
5. Zhu F, Zykova TA, Kang BS, Wang Z, Ebeling MC, Abe Y, Ma W–Y, Bode AM, Dong Z (2007) Bidirectional signals transduced by TOPK-ERK interaction increase tumorigenesis of HCT116 colorectal cancer cells. Gastroenterology 133:219–231
6. Hu F, Gartenhaus RB, Zhao XF, Fang HB, Minkove S, Poss DE, Rapoport AP (2013) C-Myc and E2F1 drive PBK/TOPK expression in high-grade malignant lymphomas. Leuk Res 37:447–454
7. Simons-Evelyn M, Bailey-Dell K, Toretsky JA, Ross DD, Fenton R, Kalvakolanu D, Rapoport AP (2001) PBK/TOPK is a novel mitotic kinase which is upregulated in Burkitt's lymphoma and other highly proliferative malignant cells. Blood Cells Mol Dis 27:825–829
8. Ikeda Y, Park J-H, Miyamoto T, Takamatsu N, Kato T, Iwasa A, Okabe S, Imai Y, Fujiwara K, Nakamura Y, Hasegawa K (2016) T-LAK cell-originated protein kinase (TOPK) as a prognostic factor and a potential therapeutic target in ovarian Cancer. Clin Cancer Res 22:6110–6117
9. Lei B, Qi W, Zhao Y, Li Y, Liu S, Xu X, Zhi C, Wan L, Shen H (2015) PBK/TOPK expression correlates with mutant p53 and affects patients' prognosis and cell proliferation and viability in lung adenocarcinoma. Hum Pathol 46:217–224
10. Shih MC, Chen JY, Wu YC, Jan YH, Yang BM, Lu PJ, Cheng HC, Huang MS, Yang CJ, Hsiao M, Lai JM (2012) TOPK/PBK promotes cell migration via modulation of the PI3K/PTEN/AKT pathway and is associated with poor prognosis in lung cancer. Oncogene 31:2389–2400
11. Stangeland B, Mughal AA, Grieg Z, Sandberg CJ, Joel M, Nygård S, Meling T, Murrell W, Vik Mo EO, Langmoen IA (2015) Combined expressional analysis, bioinformatics and targeted proteomics identify new potential therapeutic targets in glioblastoma stem cells. Oncotarget 6:26192–26215
12. Quan C, Xiao J, Duan Q, Yuan P, Xue P, Lu H, Yan M, Guo D, Xu S, Zhang X, Lin X, Wang Y, Dogan S, Zhang J, Zhu F, Ke C, Liu L (2018) T-lymphokine-activated killer cell-originated protein kinase (TOPK) as a prognostic factor and a potential therapeutic target in glioma. Oncotarget 9:7782–7795
13. Brown-Clay JD, Shenoy DN, Timofeeva O, Kallakury BV, Nandi AK, Banerjee PP (2015) PBK/TOPK enhances aggressive phenotype in prostate cancer via β-catenin-TCF/LEF-mediated matrix metalloproteinases production and invasion. Oncotarget 6:15594–15609
14. Sun H, Zhang L, Shi C, Hu P, Yan W, Wang Z, Duan Q, Lu F, Qin L, Lu T, Xiao J, Wang Y, Zhu F, Shao C (2015) TOPK is highly expressed in circulating tumor cells, enabling metastasis of prostate cancer. Oncotarget 6:12392–12404
15. Zlobec I, Molinari F, Kovac M, Bihl MP, Altermatt HJ, Diebold J, Frick H, Germer M, Horcic M, Montani M, Singer G, Yurtsever H, Zettl A, Terracciano L, Mazzucchelli L, Saletti P, Frattini M, Heinimann K, Lugli A (2010) Prognostic and predictive value of TOPK stratified by KRAS and BRAF gene alterations in sporadic, hereditary and metastatic colorectal cancer patients. Br J Cancer 102:151–161
16. Park JH, Nishidate T, Nakamura Y, Katagiri T (2010) Critical roles of T-LAK cell-originated protein kinase in cytokinesis. Cancer Sci 101:403–411
17. Zou J, Kuang W, Hu J, Rao H (2017) miR-216b promotes cell growth and enhances chemosensitivity of colorectal cancer by suppressing PDZ-binding kinase. Biochem Biophys Res Commun 488:247–252
18. Pirovano G, Ashton TM, Herbert KJ, Bryant RJ, Verrill CL, Cerundolo L, Buffa FM, Prevo R, Harrap I, Ryan AJ, Macaulay V, McKenna WG, Higgins GS (2017) TOPK modulates tumour-specific radiosensitivity and correlates with recurrence after prostate radiotherapy. Br J Cancer 117:503–512
19. Shats I, Gatza ML, Chang JT, Mori S, Wang J, Rich J, Nevins JR (2011) Using a stem cell-based signature to guide therapeutic selection in cancer. Cancer Res 71:1772–1780
20. Matsumoto S, Abe Y, Fujibuchi T, Takeuchi T, Kito K, Ueda N, Shigemoto K, Gyo K (2004) Characterization of a MAPKK-like protein kinase TOPK. Biochem Biophys Res Commun 325:997–1004
21. Kim DJ, Li Y, Reddy K, Lee MH, Kim MO, Cho YY, Lee SY, Kim JE, Bode AM, Dong Z (2012) Novel TOPK inhibitor HI-TOPK-032 effectively suppresses colon cancer growth. Cancer Res 72:3060–3068
22. Matsuo Y, Park JH, Miyamoto T, Yamamoto S, Hisada S, Alachkar H, Nakamura Y (2014) TOPK inhibitor induces complete tumor regression in xenograft models of human cancer through inhibition of cytokinesis. Sci Transl Med 6:259ra145
23. Gao G, Zhang T, Wang Q, Reddy K, Chen H, Yao K, Wang K, Roh E, Zykova T, Ma W, Ryu J, Curiel-Lewandrowski C, Alberts D,

Dickinson SE, Bode AM, Xing Y, Dong Z (2017) ADA-07 suppresses solar ultraviolet-induced skin carcinogenesis by directly inhibiting TOPK. Mol Cancer Ther 16:1843–1854

24. Zeng X, Liu L, Zheng M, Sun H, Xiao J, Lu T, Huang G, Chen P, Zhang J, Zhu F, Li H, Duan Q (2016) Pantoprazole, an FDA-approved proton-pump inhibitor, suppresses colorectal cancer growth by targeting T-cell-originated protein kinase. Oncotarget 7:22460–22473
25. Zheng M, Luan S, Gao S, Cheng L, Hao B, Li J, Chen Y, Hou X, Chen L, Li H (2017) Proton pump inhibitor ilaprazole suppresses cancer growth by targeting T-cell-originated protein kinase. Oncotarget 8:39143–39153
26. Nakamura Y, Matsuo Y, Hisada S et al (2016) Tricyclic compounds and pbk inhibitors containing the same. OncoTherapy science, Inc., Kanagawa, Japan
27. Sugimori M, Hayakawa Y, Koh M, Hayashi T, Tamura R, Kuroda S (2018) Targeting the T-Lak cell originated protein kinase by OTS964 shrinks the size of power-law coded heterogeneous glioma stem cell populations. Oncotarget 9:3043–3059
28. Kniess T, Laube M, Brust P, Steinbach J (2015) 2-[^{18}F]Fluoroethyl tosylate – a versatile tool for building ^{18}F-based radiotracers for positron emission tomography. Med Chem Commun 6:1714–1754